Acta Crystallographica Section A
Foundations of Crystallography
ISSN 0108-7673

Received 16 May 2013
Accepted 31 July 2013

C_{70}, C_{80}, C_{90} and carbon nanotubes by breaking of the icosahedral symmetry of C_{60}

Mark Bodner,[a] Jiří Patera[a,b] and Marzena Szajewska[b,c]*

[a]MIND Research Institute, 111 Academy Drive, Irvine, California 92617, USA, [b]Centre de Recherches Mathématiques, Université de Montréal, C. P. 6128, Centre-ville, Montréal, H3C 3J7, Québec, Canada, and [c]Institute of Mathematics, University of Bialystok, Akademicka 2, PL-15-267, Bialystok, Poland. Correspondence e-mail: m.szajewska@math.uwb.edu.pl

The icosahedral symmetry group H_3 of order 120 and its dihedral subgroup H_2 of order 10 are used for exact geometric construction of polytopes that are known to exist in nature. The branching rule for the H_3 orbit of the fullerene C_{60} to the subgroup H_2 yields a union of eight orbits of H_2: four of them are regular pentagons and four are regular decagons. By inserting into the branching rule one, two, three or n additional decagonal orbits of H_2, one builds the polytopes C_{70}, C_{80}, C_{90} and nanotubes in general. A minute difference should be taken into account depending on whether an even or odd number of H_2 decagons are inserted. Vertices of all the structures are given in exact coordinates relative to a non-orthogonal basis naturally appropriate for the icosahedral group, as well as relative to an orthonormal basis. Twisted fullerenes are defined. Their surface consists of 12 regular pentagons and 20 hexagons that have three and three edges of equal length. There is an uncountable number of different twisted fullerenes, all with precise icosahedral symmetry. Two examples of the twisted C_{60} are described.

1. Introduction

Some three decades ago stable carbon molecules C_{60} and C_{70} were discovered. This stimulated a large number of studies, both experimental and theoretical, involving such molecules and their modifications (Dresselhaus *et al.*, 1996; Fowler & Manolopoulos, 2007; Harris, 1999; Keef & Twarock, 2009; Twarock, 2002) under the generic name 'fullerenes'. More fullerenes were found to exist in nature and many more pentagon/hexagon shells are described in the literature (Dresselhaus *et al.*, 1996; Fowler & Manolopoulos, 2007; Harris, 1999; Kroto & Walton, 1993).

The C_{60}[1] molecule is the most common member of the family of hollow-cage carbon cluster fullerenes. The C_{60} molecule has been investigated experimentally in the solid state as well as in the gas phase (Cataldo *et al.*, 2010; Dresselhaus *et al.*, 1996; Shinar *et al.*, 1999; Verberck & Michel, 2007). The structure of C_{60} is that of a truncated icosahedron, made of hexagons and pentagons, with 60 carbon atoms positioned at vertices of the corners of the hexagons, and a bond along each edge. The next most common naturally occurring member of the hollow-cage cluster fullerenes is composed of 70 carbon atoms and is the molecule C_{70}, possessing a rugby-ball structure with a slight pinching at its waist as the bond lengths follow a simple pattern determined by their relationship to five- and six-membered rings (McKenzie *et al.*, 1992; Randic & Vukicevic, 2006).

A significant amount of effort has taken place to determine the reasons for the stability of the C_{60} and C_{70} molecules, as well as towards ascertaining which other fullerenes, of different size and form, can be produced as stable entities. A number of closed-cage fullerenes with greater than 70 carbon atoms have now been experimentally produced and confirmed to exist, while calculations have predicted that all even-numbered fullerenes with size greater than C_{70} may be theoretically possible.

One aim of this paper is to provide exact descriptions of particular fullerenes. Such a construction could enable, for example, defining functions on them leading to useful further studies. In particular, let us imagine, for example, a function of $x \in \mathbb{R}^3$ defined by a particular fullerene in the following way. Each vertex contributes to such a fullerene function $\exp(2\pi i\langle\lambda, x\rangle)$, where the scalar product contains the coordinates λ of the vertex and the continuous variable x is in $\mathbb{R}^3$. In terms of different fullerene functions one could study interactions between carbon atoms and interactions with the field generated by the fullerene in the entire space $\mathbb{R}^3$. Clearly knowing the position of vertices of the fullerene with limited precision would handicap such a study. The construction with exact coordinates is accomplished in this work through the breaking of the icosahedral symmetry to one of its maximal subgroups. In the present work, that subgroup is H_2, the dihedral group of order 10.

[1] C_{60} is a standard symbol for the polytope commonly used to model certain carbon molecules.

It turns out that little information can be found in the literature about the exact coordinates of vertices of fullerenes with broken icosahedral symmetry. Typically one would be referred to classical polytopes, or to detailed information provided about conjugacy classes of the elements of the icosahedral group (Dresselhaus *et al.*, 1996; Li & Xu, 2009). But these two refer only to structures confined to a sphere.

The task of providing exact coordinates of all vertices of the fullerenes is possible, provided one uses appropriate bases related to the icosahedral group even when the symmetry is broken to a subgroup of H_3.[2] Those are the bases of simple roots of H_3, the α-basis, and its dual, the ω-basis, or their combination. If an orthonormal basis needs to be used, there is a particular choice that allows one to have exact coordinates of the vertices (Chen *et al.*, 1998; Conway & Sloane, 1998; Moody & Patera, 1993). Such an orthonormal basis in $\mathbb{R}^3$ can be understood as formed by a discrete set of purely imaginary quaternions ('icosians') (Moody & Patera, 1993). A role for the quaternionic multiplication of the discrete set of vectors-roots of H_3 is yet to be found in fullerene studies.

In the present work we consider the existence and structure of fullerenes larger than C_{60} as a symmetry-breaking problem. Guided by the common practice in particle physics, we consider the description specifically of the C_{70}, C_{80} and C_{90} molecules as a symmetry-breaking problem with the additional twist that the usual branching rule H_3 to H_2 is enhanced by adding to it an additional decagonal H_2 term. The group H_2 is the lowest non-crystallographic finite reflection group, known as the dihedral group of order 10. We consider the icosahedral group H_3 of order 120 of the fullerene C_{60} as the exact symmetry that is broken to its subgroup H_2 of order 10 of dihedral symmetries. We also show within this framework, utilizing this symmetry-breaking mechanism, how more complex fullerene structures, such as nanotubes, may naturally arise. This provides a framework for understanding the occurrence of a number of even-numbered fullerenes and more complex structures may be assembled.

In §2 the icosahedral symmetry of C_{60} is recalled and pertinent tools for the subsequent consideration are introduced. In §3 the vertices of C_{60} are generated and examples of its surface features are described. In §4 the structure of C_{60} is viewed from its subgroup H_2. In §5 the structures of C_{70} and also C_{80} are presented.

In the last section we describe a continuum of 'twisted fullerenes' with exact icosahedral symmetry, apparently not found in the fullerene-related literature. The polytope C_{60} is just one member of the continuum of possibilities. By working out two particular examples, we show other members of the set of polytopes with exact icosahedral symmetry.

[2] Contemporary theory of finite reflection groups is an accomplished part of mathematics, where the notations H_2, H_3, H_4 are standard names of non-crystallographic reflection groups in two-, three- and four-dimensional Euclidean spaces.

2. Icosahedral symmetry of C_{60}

The icosahedral symmetry has been known from antiquity. The icosahedral symmetry group has been presented since then in various degrees of completeness, complexity and abstraction (see example in Litvin, 1991). If extensive computations are to be undertaken using the icosahedral group or any other finite reflection group in Euclidean space, then the approach that starts from the corresponding Coxeter–Dynkin diagram of simple roots is the most efficient and thus the most practical one (Humphreys, 1990). This is the path we use here. At the outset the theory provides one with

(i) the simple roots that are the normals to the reflection mirrors for the corresponding reflection group [equation (1)];

(ii) the dual or reciprocal ω-basis [equation (4)];

(iii) the general formula [equation (9)] for reflections in any Euclidean space.

In this section we work out the details for these three sets of tools pertaining to the icosahedral symmetry.

First let us introduce the solutions of the quadratic equation $x^2 = x + 1$:

$$\tau = \frac{1}{2}(1 + 5^{1/2}) \simeq 1.6180\ldots,$$
$$\tau' = \frac{1}{2}(1 - 5^{1/2}) = 1 - \tau = -1/\tau \simeq -0.6180\ldots,$$

where τ is known as the golden mean.

All coordinates of the vertices of C_{60}, C_{70} and related fullerenes and nanotubes are given here in non-orthogonal bases inherent to the icosahedral symmetry group. An option is also presented which allows one to rewrite the vertices using exact coordinates in an orthonormal basis of the three-dimensional real Euclidean space $\mathbb{R}^3$. The coordinates relative to all such bases are exact and all are of the form $\mathbb{Q} + \mathbb{Q}\tau$, where $\mathbb{Q}$ stands for a rational number.

2.1. Three useful bases in $\mathbb{R}^3$

Besides the orthonormal basis in the three-dimensional real Euclidean space $\mathbb{R}^3$, it is useful to introduce a pair of dual bases directly related to the icosahedral symmetry. However, even the orthogonal basis can be introduced in a way particularly appropriate for the finite non-crystallographic Coxeter groups (Chen *et al.*, 1998; Moody & Patera, 1993). Among those groups the group H_3 is the second largest, see §2.4.

2.2. The α-basis $\{\alpha_1, \alpha_2, \alpha_3\}$

The simple root basis exists for every finite group generated by reflections (Deodhar, 1982) and, in particular, also for the icosahedral group H_3 of order 120 (Chen *et al.*, 1998; Moody & Patera, 1993). The lengths and relative angles of the α-basis of $\mathbb{R}^3$ are defined by the matrix C of the scalar products of the basis vectors

$$C = (C_{jk}) = (\langle \alpha_j, \alpha_k \rangle) = \begin{pmatrix} 2 & -1 & 0 \\ -1 & 2 & -\tau \\ 0 & -\tau & 2 \end{pmatrix},$$
$$\det C = 6 - 2\tau^2 = 4 - 2\tau \simeq 0.7749\ldots. \quad (1)$$

The α-basis is conveniently shown as the nodes of the Coxeter diagram of H_3 on Fig. 1. Decorations of the links between the nodes of the diagram imply the following values of the scalar products:

$$\langle \alpha_1, \alpha_2 \rangle = -1, \qquad \langle \alpha_2, \alpha_3 \rangle = -\tau, \qquad \langle \alpha_1, \alpha_3 \rangle = 0. \quad (2)$$

Note that, according to equation (1), the basis vectors are of the same length, namely $2^{1/2}$.

2.3. The ω-basis $\{\omega_1, \omega_2, \omega_3\}$

The relative angles and lengths of the vectors of the ω-basis are defined by the matrix C^{-1} inverse to C. The matrix C^{-1} is formed by the scalar products of the basis vectors

$$(C_{jk}^{-1}) = (\langle \omega_j, \omega_k \rangle) = \frac{1}{\det C} \begin{pmatrix} 3-\tau & 2 & \tau \\ 2 & 4 & 2\tau \\ \tau & 2\tau & 3 \end{pmatrix} = \frac{1}{2} \begin{pmatrix} 2+\tau & 2+2\tau & 1+2\tau \\ 2+2\tau & 4+4\tau & 2+4\tau \\ 1+2\tau & 2+4\tau & 3+3\tau \end{pmatrix}. \quad (3)$$

Note that the vectors ω_1, ω_2 and ω_3 are of different length.

The duality of the bases

$$\langle \alpha_j, \omega_k \rangle = \delta_{jk}, \qquad j, k = 1, 2, 3 \quad (4)$$

is a consequence of their definitions. Indeed, we have the matrix relations

$$\alpha = C\omega, \qquad \omega = C^{-1}\alpha. \quad (5)$$

The dihedral subgroup of H_3, which is of order 10, is denoted here by H_2. For its simple roots we choose two of the simple roots of H_3, namely α_2 and α_3. By equation (4), the direction orthogonal to the H_2 plane, spanned by ω_2 and ω_3, is that of α_1. The mixed basis of $\{\alpha_1, \omega_2, \omega_3\}$ turns out to be useful to us subsequently.

2.4. The α- and ω-bases of H_3 in coordinates relative to an orthonormal basis

The root system of H_3 consists of 30 roots. Its 15 positive roots are listed in equation (6.13) of Champagne *et al.* (1995) as a linear combination of the simple roots. The simple roots of H_3 can be chosen (Chen *et al.*, 1998; Conway & Sloane, 1998; Moody & Patera, 1993) relative to an orthonormal basis in a real Euclidean space $\mathbb{R}^3$ of dimension 3 as follows:

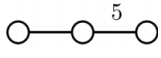

Figure 1
Coxeter diagram of H_3. Its nodes are taken to stand either for the basis vectors of the α-basis numbered from left to right, or for the vectors of the ω-basis, or for the reflections r_1, r_2, r_3 in mirrors orthogonal to vectors of the α-basis and intersecting at the origin of $\mathbb{R}^3$.

$$\alpha_1 = \frac{1}{2^{1/2}}(-\tau', -\tau, 1), \quad \alpha_2 = \frac{1}{2^{1/2}}(1, -\tau', -\tau),$$
$$\alpha_3 = \frac{1}{2^{1/2}}(-1, -\tau', \tau), \quad (6)$$

where the constant $2^{1/2}$ is to maintain the normalization of the simple roots as in equation (1). The highest root of H_3 is $-\tau'\omega_2$.

The ω-basis of H_3 is found relative to the α-basis using equation (5), and relative to the orthonormal basis using equations (5) and (6):

$$\omega_1 = \frac{1}{2}[(2+\tau)\alpha_1 + (2+2\tau)\alpha_2 + (1+2\tau)\alpha_3] = \frac{1}{2^{1/2}}(\tau, 0, 1)$$
$$\omega_2 = \frac{1}{2}[(2+2\tau)\alpha_1 + (4+4\tau)\alpha_2 + (2+4\tau)\alpha_3] = \frac{1}{2^{1/2}}(1+\tau, \tau, 1)$$
$$\omega_3 = \frac{1}{2}[(1+2\tau)\alpha_1 + (2+4\tau)\alpha_2 + (3+3\tau)\alpha_3] = \frac{1}{2^{1/2}}\tau(1, 1, 1). \quad (7)$$

2.5. The reflections generating the icosahedral group

The three reflection operations, r_1, r_2 and r_3, in $\mathbb{R}^3$ that satisfy the identities

$$r_1^2 = r_2^2 = r_3^2 = 1, \quad (r_1 r_2)^3 = 1, \quad (r_1 r_3)^2 = 1, \quad (r_2 r_3)^5 = 1 \quad (8)$$

define abstractly (Chen *et al.*, 1998; Humphreys, 1990) the icosahedral group H_3 of order 120. Explicitly one has

$$r_k x = x - \langle x, \alpha_k \rangle \alpha_k, \qquad k = 1, 2, 3, \qquad x \in \mathbb{R}^3. \quad (9)$$

Any point $x \in \mathbb{R}^3$ is reflected by r_k in the mirror orthogonal to α_k and passing through the origin of $\mathbb{R}^3$. In particular, $r_k 0 = 0$, $r_k \alpha_k = -\alpha_k$ and $r_k \omega_j = \omega_j - \alpha_j \delta_{jk}$. The points x and $r_k x$ are equidistant from the origin of $\mathbb{R}^3$.

2.6. The facets of C_{60}

The facets of C_{60} of dimensions 0, 1, 2 are, respectively, 60 vertices, 90 edges, 32 faces out of which 20 are hexagons and 12 are pentagons (Fig. 2).

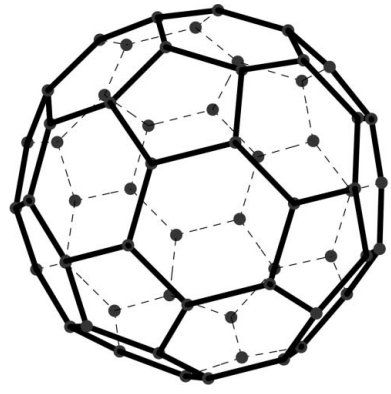

Figure 2
The polytope C_{60} is formed by 60 vertices equidistant from its centre. Its surface consists of 12 regular pentagons and 20 regular hexagons. All 90 edges are of the same length.

There is a little-known efficient method (Champagne *et al.*, 1995; Szajewska, 2012) for describing the representative faces of any polytope generated by reflection in $\mathbb{R}^n$. In particular, it allows one to count the number of faces of C_{60} and it makes straightforward construction of a representative face of each conjugacy class. The method consists in recursively decorating[3] the corresponding diagram and reading off the decoration the reflections generating the symmetry group of each face (black lozenges) and the stabilizer of the face (white lozenges). The number of faces in each of the H_3 orbit/conjugacy classes is obtained by dividing the order of H_3 by the order of the symmetry group of the face multiplied by the order of the stabilizer of the face. For more details about the recursive decorations of the diagram on Fig. 1, see Champagne *et al.* (1995). Applied to the fullerene, we get the following decorations of the diagram Fig. 1. Each decoration refers to one conjugacy class of faces of the polytope C_{60}.

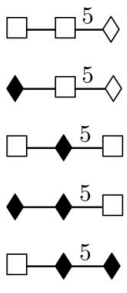

$120/2 = 60$	vertices	(a)
$120/4 = 30$	hexagon-hexagon edges	(b)
$120/2 = 60$	pentagon-hexagon edges	(c)
$120/6 = 20$	hexagons	(d)
$120/10 = 12$	pentagons	(e)

The first column contains decorated nodes of the diagram of H_3. Line (a) in the scheme refers to the vertices. All belong to the same H_3 conjugacy class; equivalently, they are generated by the reflections from the same seed point $(1, 1, 0) = \omega_1 + \omega_2$. Line (b) in the scheme counts the edges where two hexagonal faces meet. Similarly line (c) in the scheme counts the edges that separate hexagonal and pentagonal faces. In lines (d) and (e) in the scheme the hexagonal and the pentagonal faces of C_{60} are counted.

Note that the dimension of a face is equal to the number of black lozenges in the decoration of its diagram. Reflections corresponding to black lozenges generate the symmetry group of the face. The white lozenges indicate the reflections that fix the face pointwise.

Let us calculate and compare the lengths of the two types of edges of C_{60}, namely lines (b) and (c). Since all vertices are the same, we calculate the lengths between the seed point [line (a)], which is $\omega_1 + \omega_2$ and $r_1(\omega_1 + \omega_2)$ in one case, and $\omega_1 + \omega_2$ and $r_2(\omega_1 + \omega_2)$ in the other case. In order to simplify the expressions, we leave out the angle brackets of the scalar products. Scalar products of vectors of ω-basis are read off equation (3),

$$\{[\omega_1 + \omega_2 - r_1(\omega_1 + \omega_2)]^2\}^{1/2} = [(2\omega_1 - \omega_2)^2]^{1/2} = 2^{1/2}.$$

Similarly

$$\{[\omega_1 + \omega_2 - r_2(\omega_1 + \omega_2)]^2\}^{1/2} = [(-\omega_1 + 2\omega_2 - \tau\omega_3)^2]^{1/2} = 2^{1/2}.$$

The hexagonal faces of C_{60} emerge naturally from the classification of its 2-faces as one orbit of the seed hexagon [line (d)]. The symmetry group of the hexagons is generated by the reflections r_1 and r_2. Similarly the pentagon faces of C_{60} come up naturally from the classification of its 2-faces as one orbit of the seed pentagon [line (e)]. The symmetry group of the pentagons is generated by the reflections r_2 and r_3.

Let us illustrate the construction of the hexagons and of the pentagon that have in common the dominant point of C_{60}:

$$\begin{aligned}
&(1, 1, 0)\\
r_1(1, 1, 0) &= (-1, 2, 0)\\
r_2(1, 1, 0) &= (2, -1, \tau)\\
r_1r_2(1, 1, 0) &= (-2, 1, \tau)\\
r_3r_2r_1(1, 1, 0) &= (1, -2, 2\tau)\\
r_1r_2r_1(1, 1, 0) &= (-1, -1, 2\tau) \qquad (10a)
\end{aligned}$$

$$\begin{aligned}
&(1, 1, 0)\\
r_2(1, 1, 0) &= (2, -1, \tau)\\
r_3r_2(1, 1, 0) &= (2, \tau, -\tau)\\
r_2r_3r_2(1, 1, 0) &= (2 + \tau, -\tau, 1)\\
r_3r_2r_3r_2(1, 1, 0) &= (2 + \tau, 0, -1) \qquad (10b)
\end{aligned}$$

$$\begin{aligned}
r_3(1, 1, 0) &= (1, 1, 0)\\
r_3r_1(1, 1, 0) &= (-1, 2, 0)\\
r_3r_2(1, 1, 0) &= (2, \tau, -\tau)\\
r_3r_1r_2(1, 1, 0) &= (-2, 2 + \tau, -\tau)\\
r_3r_2r_1(1, 1, 0) &= (1, 2\tau, -2\tau)\\
r_3r_1r_2r_1(1, 1, 0) &= (-1, 1 + 2\tau, -2\tau). \qquad (10c)
\end{aligned}$$

The vertices of a hexagon and pentagon of the surface of C_{60} adjacent to the dominant point of C_{60} are shown here in the ω-basis. The pentagon of equation $(10b)$ is situated in the plane spanned by ω_2 and ω_3. Therefore it is generated by the reflections r_2 and r_3. The first hexagon of equation $(10a)$ is situated in the plane spanned by ω_1 and ω_2. Therefore it is generated by reflections r_1 and r_2. The second hexagon is situated in a plane that is not the same as the plane of the first hexagon. It is the first hexagon transformed point-by-point by r_3.

The seed point $(1, 1, 0)$ is a vertex shared by three faces of dimension 2 of C_{60}. In equations $(10a)$, $(10b)$, $(10c)$ we have constructed the pentagon and both hexagons.

3. The vertices of C_{60}

Fig. 2 shows the polytope of C_{60}. It is colloquially called fullerene or buckyball, soccerball or even soccerballene. The vertices of C_{60} are generated by the reflections [equation (9)] from any of its points. Therefore they all belong to the same H_3 orbit. The list [equation (11)] of vertices of C_{60} is given in the ω-basis of §2.3. It is a non-orthogonal basis [*cf.* equation (3)] defined for the icosahedral symmetry. Therefore the

[3] There is a 1–1 correspondence between symbols used to decorate the Coxeter–Dynkin diagrams here and in previous papers. More precisely, the black lozenge, square, white lozenge symbols correspond, respectively, to the circled dot, square, crossed box, in Moody & Patera (1992), Moody & Patera (1995) and to the circle, square, crossed box in Champagne *et al.* (1995).

important properties of the polytope are read directly from the list [equation (11)] where the vertices are given in the ω-basis.

Each entry in equation (11) carries both signs, *i.e.* stands for two diametral points. It is practical to start the sequence of reflections, generating the vertices of the polytope, from the 'dominant' point of the orbit. It is the unique point of the orbit that has non-negative coordinates in the ω-basis. The dominant point of C_{60} is $(1, 1, 0) = \omega_1 + \omega_2$. All 60 vertices of C_{60} are shown in equation (11). The points written in bold have the second and the third coordinates with the same sign:

$$
\begin{array}{lll}
\pm(\mathbf{1}, \mathbf{1}, \mathbf{0}) & \pm(-\mathbf{2}, \mathbf{1}, \boldsymbol{\tau}) & \pm(-1, -1, 2\tau) \\
 & \pm(2, -1, \tau) & \pm(1, -2, 2\tau) \\
\pm(-\mathbf{1}, \mathbf{2}, \mathbf{0}) & \pm(\mathbf{1} + \mathbf{2}\boldsymbol{\tau}, \mathbf{0}, -\mathbf{2}) & \pm(2 + \tau, -\tau, 1) \\
 & \pm(1, 2\tau, -2\tau) & \pm(-1, 1 + 2\tau, -2\tau) \\
\pm(-\mathbf{2} - \boldsymbol{\tau}, \mathbf{2}, \mathbf{1}) & \pm(\tau, -2 - \tau, 1 + 2\tau) & \pm(-\tau, -2, 1 + 2\tau) \\
 & \pm(1 + 2\tau, -2\tau, 2) & \pm(2\tau, -1 - 2\tau, 2 + \tau) \\
\pm(\mathbf{2} + \boldsymbol{\tau}, \mathbf{0}, -\mathbf{1}) & \pm(\tau, 2\tau, -1 - 2\tau) & \pm(-2 - \tau, 2 + \tau, -1) \\
 & \pm(-2, 2 + \tau, -\tau) & \pm(-2\tau, -1, 2 + \tau) \\
\pm(-\mathbf{1} - \mathbf{2}\boldsymbol{\tau}, \mathbf{1}, \mathbf{2}) & \pm(2\tau, \tau, -2 - \tau) & \pm(-\tau, 3\tau, -1 - 2\tau) \\
 & \pm(3\tau, -2\tau, 1) & \pm(0, -2 - \tau, 3\tau) \\
\pm(\mathbf{3}\boldsymbol{\tau}, -\boldsymbol{\tau}, -\mathbf{1}) & \pm(-1 - 2\tau, 1 + 2\tau, -2) & \pm(-2\tau, 3\tau, -2 - \tau) \\
 & \pm(0, 1 + 2\tau, -3\tau) & \pm(2, \tau, -\tau).
\end{array}
\tag{11}
$$

There are pairs of opposite points that are given in bold. Such points are selected because their second and third coordinates have the same sign. One of the two points with non-negative coordinates is the dominant point of an H_2 orbit. Every H_2 orbit contains precisely one dominant point. If both coordinates are strictly positive, the orbit is a decagon. If one of them is zero, the orbit is a pentagon. The point with both the second and third coordinates zero would be on the α_1 axis, *i.e.* the H_2 orbit of one point.

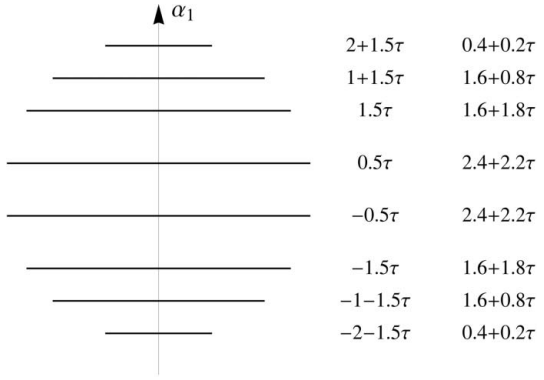

Figure 3
The C_{60} polytope viewed in the direction parallel to the H_2 plane spanned by ω_2 and ω_3. Horizontal segments are projections of the H_2 orbits. Individual vertices and edges of C_{60} are not shown. The first number in a row is the α_1 coordinate that distinguishes the H_2 orbit inside the H_3 orbit of C_{60}. The second number shows the radius of the circles containing pentagons and decagons. The vertical direction is that of α_1.

4. The H_2 structure of C_{60}

Let us underline that one needs to distinguish pentagons that are the faces of C_{60} and the H_2 pentagons in planes orthogonal to the α_1 axis (Fig. 3).

In Fig. 3 one views the H_2 structure of the C_{60} polytopes as a 'stack of pancakes', *i.e.* from the direction parallel to the plane spanned by ω_2 and ω_3. That makes the H_2 orbits appear as one-dimensional segments, the 'pancakes' viewed from the side. Only the top and bottom pentagons of the stack are among the 12 pentagons that belong to the surface of C_{60}.

Reduction of the H_3 symmetry of C_{60} to that of H_2 decomposes the 60 vertices into the union of eight orbits of H_2, specified by the bold points in the list [equation (11)] of vertices of C_{60}. Out of the eight orbits, four are pentagons and four are decagons,

$$C_{60}: \quad 5 + 5 + 10 + 10 + 10 + 10 + 5 + 5, \tag{12}$$

where 5 and 10 stand for a pentagon and decagon, respectively. The decomposition is illustrated in Fig. 3.

The crucial observation one easily makes looking at Fig. 4 is that there are no pentagonal faces attached simultaneously to the upper and lower halves of C_{60}. Therefore the contact between the two halves is made by faces that are hexagons.

The four H_2 pentagons in the basis $\{\omega_1, \omega_2, \omega_3\}$ as they appear in Fig. 3 are

$$
\begin{array}{lll}
(1, 1, 0), & (2, -1, \tau), & (2, \tau, -\tau), \\
 & (2 + \tau, -\tau, 1), & (2 + \tau, 0, -1), \\
(-1, 2, 0), & (1, -2, 2\tau), & (1, 2\tau, -2\tau), \\
 & (1 + 2\tau, -2\tau, 2), & (1 + 2\tau, 0, -2), \\
(-1 - 2\tau, 0, 2), & (-1 - 2\tau, 2\tau, -2), & (-1, -2\tau, 2\tau), \\
 & (-1, 2, -2\tau), & (1, -2, 0), \\
(-2 - \tau, 0, 1), & (-2 - \tau, \tau, -1), & (-2, -\tau, \tau), \\
 & (-2, 1, -\tau), & (-1, -1, 0)
\end{array}
\tag{13}
$$

and the same pentagons in the basis $\{\alpha_1, \omega_2, \omega_3\}$,

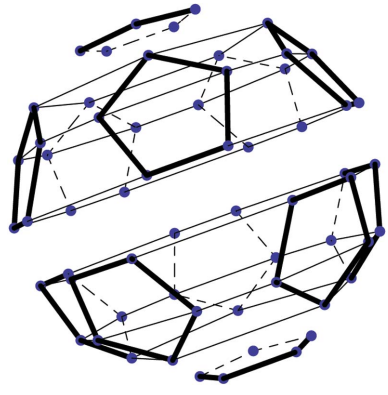

Figure 4
The C_{60} polytope oriented as in Fig. 2. The 12 pentagons of the surface of C_{60} are shown without the hexagons. The 60 dots are the vertices of C_{60}.

$$
\begin{array}{lll}
(2+\tfrac{3\tau}{2},1,0) & (2+\tfrac{3\tau}{2},-1,\tau), & (2+\tfrac{3\tau}{2},\tau,-\tau),\\
 & (2+\tfrac{3\tau}{2},-\tau,1), & (2+\tfrac{3\tau}{2},0,-1),\\
(1+\tfrac{3\tau}{2},2,0), & (1+\tfrac{3\tau}{2},-2,2\tau), & (1+\tfrac{3\tau}{2},2\tau,-2\tau),\\
 & (1+\tfrac{3\tau}{2},-2\tau,2), & (1+\tfrac{3\tau}{2},0,-2),\\
(-1-\tfrac{3\tau}{2},0,2), & (-1-\tfrac{3\tau}{2},2\tau,-2), & (-1-\tfrac{3\tau}{2},-2\tau,2\tau),\\
 & (-1-\tfrac{3\tau}{2},2,-2\tau), & (-1-\tfrac{3\tau}{2},-2,0),\\
(-2-\tfrac{3\tau}{2},0,1), & (-2-\tfrac{3\tau}{2},\tau,-1), & (-2-\tfrac{3\tau}{2},-\tau,\tau),\\
 & (-2-\tfrac{3\tau}{2},1,-\tau), & (-2-\tfrac{3\tau}{2},-1,0).
\end{array}
\tag{14}
$$

The four pentagons of equation (13) and of equation (14) split into two pairs. Within each pair the pentagons differ by permutation of the second and third coordinates, *i.e.* they have opposite orientations in the plane spanned by ω_2 and ω_3, and in equation (14) the α_1 coordinates have opposite signs within each pair.

Between the top two pentagons (see Fig. 3) and bottom two pentagons, there are four H_2 decagons. On the surface of C_{60} there is a ring of hexagons that connects the upper and lower parts of the polytope. Unwrapping that ring into a plane, one gets the ten hexagons of Fig. 5. Horizontal lines in Fig. 5 indicate the position of the four H_2 decagons. The dominant weights at each line specify particular decagons shown also in Fig. 3.

The ten points that are at the intersection of each line with the hexagons are the vertices of the corresponding H_2 decagon. The correspondence is established by the dominant weights shown in Fig. 5. The vertices are given relative to the basis $\{\alpha_1, \omega_2, \omega_3\}$. In particular, the first coordinate shows the position of the decagon on the α_1 axis. One may also notice that the vertices of the H_2 decagons on the four horizontal lines of Fig. 5 occur in pairs and that the pairs are shifted horizontally relative to each other.

Looking along the α_1 axis, at the four decagons of Fig. 5, when they form the ring in C_{60}, we have the ten vertices of each of the four decagons,

$$
\begin{array}{lll}
\pm(\tfrac{3\tau}{2},1,\tau), & \pm(\tfrac{3\tau}{2},-1,2\tau), & \pm(\tfrac{3\tau}{2},2+\tau,-\tau),\\
 & \pm(\tfrac{3\tau}{2},1+2\tau,-2\tau), & \pm(\tfrac{3\tau}{2},-2-\tau,1+2\tau),\\
\pm(-\tfrac{3\tau}{2},\tau,1), & \pm(-\tfrac{3\tau}{2},2\tau,-1), & \pm(-\tfrac{3\tau}{2},-\tau,2+\tau),\\
 & \pm(-\tfrac{3\tau}{2},-2\tau,1+2\tau), & \pm(-\tfrac{3\tau}{2},1+2\tau,-2-\tau)\\
\pm(\tfrac{3\tau}{2},2,1), & \pm(\tfrac{3\tau}{2},-2,1+2\tau), & \pm(\tfrac{3\tau}{2},2+\tau,-1),\\
 & \pm(\tfrac{3\tau}{2},3\tau,-1-2\tau), & \pm(\tfrac{3\tau}{2},-2-\tau,3\tau),\\
\pm(-\tfrac{3\tau}{2},1,2), & \pm(-\tfrac{3\tau}{2},1+2\tau,-2), & \pm(-\tfrac{3\tau}{2},-1,2+\tau),\\
 & \pm(-\tfrac{3\tau}{2},-1-2\tau,3\tau), & \pm(-\tfrac{3\tau}{2},3\tau,-2-\tau).
\end{array}
\tag{15}
$$

There are two pairs of the decagons which differ by permutation of the second and third coordinates indicating that they are rotated by $\frac{\pi}{10}$ degrees relative to each other.

At this stage the icosahedral symmetry is still preserved. The polytope is expressed either as one orbit of H_3 or as a union of eight orbits of H_2 that are centred at the α_1 axis and are in a plane orthogonal to it. Their position in C_{60} is given by the α_1 coordinate (see Fig. 3).

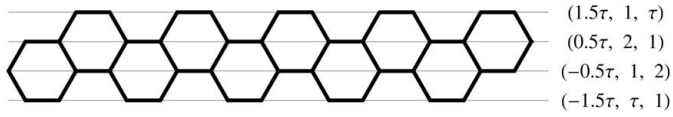

Figure 5
A ring of hexagons from the middle of the surface of C_{60} unwrapped into a plane. The dominant points identify the H_2 decagons relative to the basis $\{\alpha_1, \omega_2, \omega_3\}$. Horizontal lines indicate the H_2 decagons in the middle of C_{60} shown also in Fig. 3.

5. C_{70}

We next proceed to construct C_{70} starting from C_{60}. Inserting an additional decagon into the middle of the decomposition [equation (12)] breaks the H_3 symmetry.

5.1. Symmetry breaking

The H_3 symmetry gets broken when an additional decagon is inserted into the middle of the decomposition [equation (12)]. The enlarged structure of C_{70} loses its spherical symmetry, has 70 vertices/carbon molecules, and in the middle of it there are five consecutive parallel decagons centred at the α_1 axis (see Fig. 6)

$$C_{70}: \qquad 5+5+10+10+\mathbf{10}+10+10+5+5. \tag{16}$$

Insertion of one or several H_2 decagons into the middle of the H_2 slicing as shown in Fig. 3 needs to be accompanied by two additional adjustments in order to accomplish the transformation from C_{60} to higher fullerenes.

First the distances between the decagonal orbits in the middle of the fullerene have to be the same. For that the upper and lower halves of C_{60} have to be displaced further apart. Comparing Figs. 3 and 7, the displacement is shown as the change in the α_1 coordinates of the H_2 orbits. Indeed, α_1 coordinates are increased and decreased by 0.5τ, respectively.

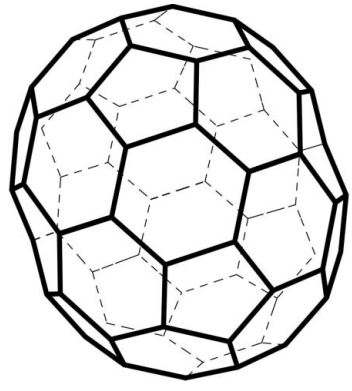

Figure 6
The polytope C_{70} has 105 edges and 12 pentagonal and 25 hexagonal faces.

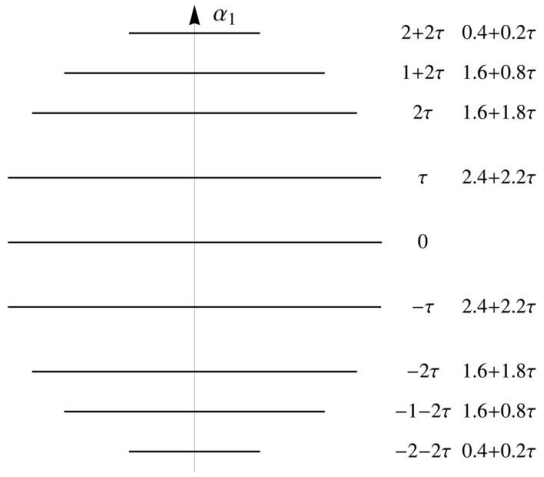

Figure 7
The H_2 orbits of C_{70} are viewed from the direction parallel to the plane of ω_2 and ω_3. The inserted decagon projects into the line in the middle.

The second adjustment refers to relative orientations of the displaced halves of C_{60}. If the number of inserted decagons is odd, like in the C_{70} case, the two halves must be mirror images of each other in order to match the surface hexagons in between them. Indeed, the top and bottom rings of hexagons in Fig. 8 are identically oriented. However, if an even number of H_2 orbits is inserted into the middle of C_{60}, the orientation of the displaced upper and lower halves of the fullerene remains the same as in C_{60} (when zero orbits are inserted). More precisely they are rotated relative to each other by $\frac{\pi}{10}$.

Finally we list the coordinates of the 70 vertices of C_{70} in the basis $\{\alpha_1, \omega_2, \omega_3\}$:

$$
\begin{array}{lll}
(\pm(\mathbf{2}+\mathbf{2\tau}), \mathbf{1}, \mathbf{0}) & (\pm(2+2\tau), -1, \tau) & (\pm(2+2\tau), \tau, -\tau) \\
 & (\pm(2+2\tau), -\tau, 1]) & (\pm(2+2\tau), 0, -1) \\
(\pm(\mathbf{1}+\mathbf{2\tau}), \mathbf{2}, \mathbf{0}) & (\pm(1+2\tau), -2, 2\tau) & (\pm(1+2\tau), 2\tau, -2\tau) \\
 & (\pm(1+2\tau), -2\tau, 2) & (\pm(1+2\tau), 0, -2) \\
(\pm\mathbf{2\tau}, \mathbf{1}, \boldsymbol{\tau}) & (\pm2\tau, -1, 2\tau) & (\pm2\tau, 2+\tau, -\tau) \\
 & (\pm2\tau, 1+2\tau, -2\tau) & (\pm2\tau, -2-\tau, 1+2\tau) \\
(\pm\boldsymbol{\tau}, \mathbf{2}, \mathbf{1}) & (\pm\tau, -2, 1+2\tau) & (\pm\tau, 2+\tau, -1) \\
 & (\pm\tau, 3\tau, -1-2\tau) & (\pm\tau, -2-\tau, 3\tau) \\
(\pm2\tau, -\tau, -1) & (\pm2\tau, -2\tau, 1) & (\pm2\tau, \tau, -2-\tau) \\
 & (\pm2\tau, 2\tau, -1-2\tau) & (\pm2\tau, -1-2\tau, 2+\tau) \\
(\pm\tau, -1, -2) & (\pm\tau, -1-2\tau, 2) & (\pm\tau, 1, -2-\tau) \\
 & (\pm\tau, 1+2\tau, -3\tau) & (\pm\tau, -3\tau, 2+\tau) \\
(\mathbf{0}, \mathbf{1}, \mathbf{2}) & (0, 1+2\tau, -2) & (0, -1, 2+\tau) \\
 & (0, -1-2\tau, 3\tau) & (0, 3\tau, -2-\tau) \\
(0, -2, -1) & (0, 2, -1-2\tau) & (0, -2-\tau, 1) \\
 & (0, -3\tau, 1+2\tau) & (0, 2+\tau, -3\tau).
\end{array}
\tag{17}
$$

Dominant points of the H_2 orbits are given in bold. In all cases but one, they come in pairs; only the orbit with its α_1 coordinate equal to 0 is unique. Altogether there are nine orbits of H_2 in C_{70}, four pentagons and five decagons.

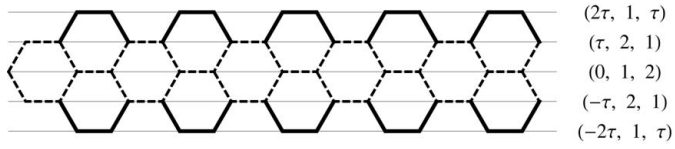

Figure 8
A ring of hexagons from the middle of the surface of C_{70} unwrapped into a plane. The horizontal lines indicate positions of the five H_2 decagons. The dominant points identify the H_2 decagons here and in Fig. 3 relative to the basis $\{\alpha_1, \omega_2, \omega_3\}$. Dashed lines are the boundaries of the ring of five inserted hexagons.

6. C_{80}, C_{90} and related nanotubes

In the same way we have inserted into the middle of C_{60} one ring of five hexagons (Fig. 8), thus forming C_{70}, one can insert two, three or more such rings, creating C_{80}, C_{90} (Fig. 9), or nanotubes of arbitrary length.

There is a fine distinction when creating such nanotubes, according to whether an even or odd number of 5-hexagon rings is inserted into C_{60}. Inserting an even number of 5-hexagon rings leaves the upper and lower halves of C_{60} intact, except for displacement along the α_1 axis to the distance required by the length of the nanotube. Inserting an odd number of 5-hexagon rings requires that the lower half of C_{60} is rotated by $\frac{\pi}{10}$ relative to its upper half, *i.e.* it becomes symmetrical with respect to the reflection r_1.

7. Twisted fullerenes

Exact icosahedral symmetry of C_{60}, which was the departure point in this paper, admits a generalization without breaking the symmetry. Among the continuum of its variants, we choose in this section just two for detailed consideration to illustrate the possibilities.

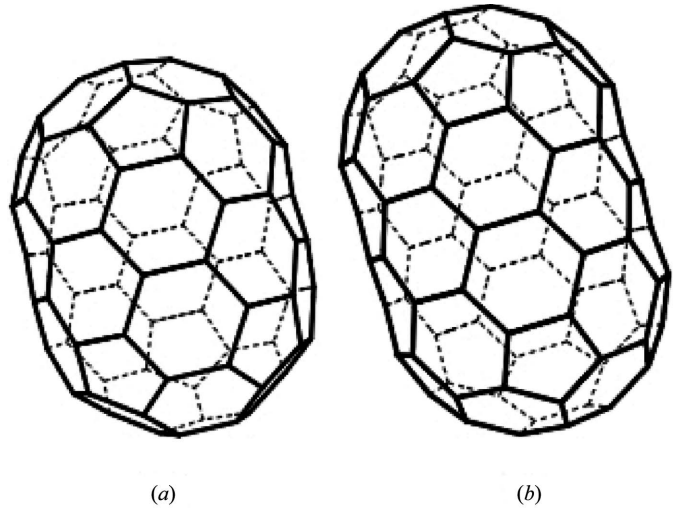

Figure 9
The polytopes (*a*) C_{80} and (*b*) C_{90}.

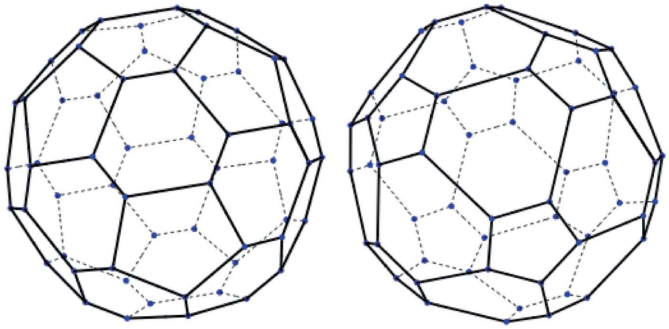

(*a*) (*b*)

Figure 10
The two cases of C_{60} which have the seed points (*a*) $\omega_1 + \tau\omega_2$ and (*b*) $\tau\omega_1 + \omega_2$.

The dominant point $\omega_1 + \omega_2$, which served as the seed point in previous sections, is replaced by

$$a\omega_1 + b\omega_2, \qquad a, b \in \mathbb{R}, \qquad a, b > 0. \tag{18}$$

The icosahedral reflections generate from the seed point the vertices of a 'twisted' C_{60}. Its 60 vertices are on a sphere of radius equal to the length of the seed point $a\omega_1 + b\omega_2$. It will have the same number of edges and 2-faces as counted in §2.6. When $a \neq b$ the hexagons cease to be regular however; three of the sides become elongated while the others are shortened. The long and short sides alternate as shown in Fig. 10. The pentagons in contrast remain regular. When either *a* or *b* vanishes the icosidodecahedron reduces to a pentagonal dodecahedron or an icosahedron, respectively. These limiting cases are well known and are of independent interest.

The two cases we consider in this section have the seed points $\omega_1 + \tau\omega_2$ and $\tau\omega_1 + \omega_2$. Icosahedral reflections r_1, r_2 and r_3 act as before, according to equation (9). One calculates the 60 vertices in the ω-basis and only then converts the results into the $\{\alpha_1, \omega_2, \omega_3\}$-basis. All 60 vertices are shown in equations (19) and (20). Bold entries with the second and third coordinates non-negative are the dominant points of the H_2 orbits. The H_2 orbits form four decagons and four pentagons in each case.

Starting from the seed point $\omega_1 + \tau\omega_2$, the reflections generate the following 60 points in the $\{\alpha_1, \omega_2, \omega_3\}$-basis:

$$\begin{array}{lll}
\pm(\mathbf{2}+\frac{5\tau}{2}, \boldsymbol{\tau}, \mathbf{0}) & \pm(\frac{\tau}{2}, \mathbf{1}+\boldsymbol{\tau}, \boldsymbol{\tau}) & \pm(2+\frac{5\tau}{2}, -\tau, 1+\tau) \\
 & \pm(1+\frac{5\tau}{2}, -1-\tau, 1+2\tau) & \pm(1+\frac{3\tau}{2}, 1+3\tau, -1-2\tau) \\
\pm(\mathbf{1}+\frac{5\tau}{2}, \mathbf{1}+\boldsymbol{\tau}, \mathbf{0}) & \pm(\mathbf{2}+\frac{5\tau}{2}, \mathbf{0}, -\boldsymbol{\tau}) & \pm(1+\frac{5\tau}{2}, 1+2\tau, -1-2\tau) \\
 & \pm(1+\frac{3\tau}{2}, 2+2\tau, -1-\tau) & \pm(2+\frac{5\tau}{2}, 1+\tau, -1-\tau) \\
\pm(\mathbf{1}+\frac{3\tau}{2}, \mathbf{1}, \mathbf{1}+\boldsymbol{\tau}) & \pm(2+\frac{5\tau}{2}, -1-\tau, \tau) & \pm(1+\frac{5\tau}{2}, -1-2\tau, 1+\tau) \\
 & \pm(1+\frac{3\tau}{2}, -2-2\tau, 1+3\tau) & \pm(1+\frac{3\tau}{2}, -1, 1+2\tau) \\
\pm(\frac{\tau}{2}, -\boldsymbol{\tau}, -\mathbf{1}-\boldsymbol{\tau}) & \pm(\frac{\tau}{2}, 2+2\tau, -\tau) & \pm(1+\frac{3\tau}{2}, -1-3\tau, 2+2\tau) \\
 & \pm(\frac{\tau}{2}, -1-\tau, 1+3\tau) & \pm(1+\frac{3\tau}{2}, 1+2\tau, -1-3\tau) \\
\pm(\mathbf{1}+\frac{5\tau}{2}, \mathbf{0}, -\mathbf{1}-\boldsymbol{\tau}) & \pm(\frac{\tau}{2}, \tau, -2-2\tau) & \pm(1+\frac{3\tau}{2}, 1+\tau, -2-2\tau) \\
 & \pm(\frac{\tau}{2}, -1-3\tau, 1+\tau) & \pm(\frac{\tau}{2}, 2+3\tau, -1-3\tau) \\
\pm(\mathbf{1}+\frac{3\tau}{2}, -\mathbf{1}-\boldsymbol{\tau}, -\mathbf{1}) & \pm(1+\frac{3\tau}{2}, -1-2\tau, 1) & \pm(\frac{\tau}{2}, -2-2\tau, 2+3\tau) \\
 & \pm(\frac{\tau}{2}, -2-3\tau, 2+2\tau) & \pm(\frac{\tau}{2}, 1+3\tau, -2-3\tau).
\end{array} \tag{19}$$

Starting from the seed point $\tau\omega_1 + \omega_2$, the reflections generate the following 60 points in the $\{\alpha_1, \omega_2, \omega_3\}$-basis:

$$\begin{array}{lll}
\pm(\frac{\mathbf{3}+\mathbf{5}\tau}{\mathbf{2}}, \mathbf{1}, \mathbf{0}) & \pm(\frac{\mathbf{3}+\mathbf{3}\tau}{\mathbf{2}}, \mathbf{1}+\boldsymbol{\tau}, \mathbf{0}) & \pm(\frac{3+5\tau}{2}, -1, \tau) \\
 & \pm(\frac{3+3\tau}{2}, -1-\tau, 1+2\tau) & \pm(\frac{3+5\tau}{2}, 1+\tau, -\tau) \\
\pm(\frac{\mathbf{1}+\mathbf{3}\tau}{\mathbf{2}}, \boldsymbol{\tau}, \boldsymbol{\tau}) & \pm(\frac{\mathbf{3}+\mathbf{3}\tau}{\mathbf{2}}, \mathbf{0}, -\mathbf{1}-\boldsymbol{\tau}) & \pm(\frac{3+3\tau}{2}, 1+2\tau, -1-2\tau) \\
 & \pm(\frac{1+3\tau}{2}, -2-2\tau, 1+2\tau) & \pm(\frac{1+3\tau}{2}, 2+2\tau, -1-2\tau) \\
\pm(\frac{\mathbf{1}+\boldsymbol{\tau}}{\mathbf{2}}, \mathbf{1}+\boldsymbol{\tau}, \boldsymbol{\tau}) & \pm(\frac{3+5\tau}{2}, -\tau, 1) & \pm(\frac{3+3\tau}{2}, -1-2\tau, 1+\tau) \\
 & \pm(\frac{1+3\tau}{2}, -1-2\tau, 2+2\tau) & \pm(\frac{1+\tau}{2}, 1+2\tau, -1) \\
\pm(\frac{\mathbf{1}+\boldsymbol{\tau}}{\mathbf{2}}, -\mathbf{1}, -\mathbf{1}-\boldsymbol{\tau}) & \pm(\frac{1+3\tau}{2}, 1+2\tau, -\tau) & \pm(\frac{1+3\tau}{2}, -\tau, 1+2\tau) \\
 & \pm(\frac{1+\tau}{2}, -1-\tau, 2+2\tau) & \pm(\frac{1+3\tau}{2}, 1+2\tau, -2-2\tau) \\
\pm(\frac{\mathbf{3}+\mathbf{5}\tau}{\mathbf{2}}, \mathbf{0}, -\mathbf{1}) & \pm(\frac{1+\tau}{2}, 1, -1-2\tau) & \pm(\frac{1+3\tau}{2}, \tau, -1-2\tau) \\
 & \pm(\frac{1+\tau}{2}, -2-2\tau, 1+\tau) & \pm(\frac{1+\tau}{2}, 1+3\tau, -2-2\tau) \\
\pm(\frac{\mathbf{1}+\mathbf{3}\tau}{\mathbf{2}}, -\boldsymbol{\tau}, -\boldsymbol{\tau}) & \pm(\frac{1+3\tau}{2}, -1-2\tau, \tau) & \pm(\frac{1+\tau}{2}, -1-2\tau, 1+3\tau) \\
 & \pm(\frac{1+\tau}{2}, -1-3\tau, 1+2\tau) & \pm(\frac{1+\tau}{2}, 2+2\tau, -1-3\tau).
\end{array} \tag{20}$$

The two cases are easily distinguished. Indeed, the case generated from the seed point $\omega_1 + \tau\omega_2$ dictates the pentagons to be larger than for the case generated from the seed point $\tau\omega_1 + \omega_2$. In addition, the edges separating two hexagons are of different length than the edges between a hexagon and pentagon.

Let us calculate the lengths of the short and long edges in both cases in Fig. 10. In order to simplify the expressions, we leave out the angle brackets of the scalar products. The value of a scalar product of two ω's is read as before from equation (3).

The length of the pentagon–hexagon edges in Fig. 10*a*:

$$\{[\omega_1 + \tau\omega_2 - r_2(\omega_1 + \tau\omega_2)]^2\}^{1/2} = \tau 2^{1/2}.$$

The length of the hexagon–hexagon edges in Fig. 10*a*:

$$\{[\omega_1 + \tau\omega_2 - r_1(\omega_1 + \tau\omega_2)]^2\}^{1/2} = [(2\omega_1 - \omega_2)^2]^{1/2} = 2^{1/2}.$$

The length of the pentagon–hexagon edges in Fig. 10*b*:

$$\{[\tau\omega_1 + \omega_2 - r_2(\tau\omega_1 + \omega_2)]^2\}^{1/2} = [(-\omega_1 + 2\omega_2 - \tau\omega_3)^2]^{1/2} = 2^{1/2}.$$

The length of the hexagon–hexagon edges in Fig. 10*b*:

$$\{[\tau\omega_1 + \omega_2 - r_1(\tau\omega_1 + \omega_2)]^2\}^{1/2} = \tau 2^{1/2}.$$

8. Fullerene special functions

Using any fullerene with known coordinates λ of its vertices, one defines fullerene functions of three real variables by placing into each vertex λ the exponential functions $\exp(2\pi i\langle\lambda, x\rangle)$, wherein the scalar product λ is multiplied with $x \in \mathbb{R}^3$. Such a function is defined by the exact coordinates of

the vertices of the particular fullerene, but it is present in the entire 3-space through its three coordinates of x.

In the special case of C_{60}, or more generally when the function is defined by a single orbit of the vertices of an H_3 polytope, the fullerene functions have many attractive properties. Most notably their products decompose into a sum of fullerene functions. However, when one is multiplying two fullerene functions where at least one has a broken H_3 symmetry, one enters a territory unexplored in the literature. As long as the H_3 symmetry is broken to one subgroup, say H_2, similar decomposition into a sum of fullerenes has to take place. No cases of such decomposition are found in the literature. At the origin of $\mathbb{R}^3$, where x is a zero vector, a fullerene function has a large maximum.

9. Concluding remarks

Precise geometric description of some of the best known fullerenes in this paper is not intended as the final word about any of them, but it can be taken as a possible departure in describing the physical properties of fullerenes. Moreover, breaking the H_3 symmetry to H_2 is just one of the avenues for icosahedral symmetry breaking that leads to fullerenes that are well known to exist in nature. There are at least two other subgroups of H_3 which could play a similar role. One is generated by the reflections r_1 and r_2, and the other is generated by r_1 and by r_3 [see equation (9)]. Such a symmetry breaking would lead to other fullerenes in an analogous way as the subgroup H_2 does here.

Exploitation of the dual 'icosahedral bases', α- and ω-bases of §§2.3 and 2.2, drastically simplifies the description of faces of C_{60} and any other polytope with H_3 symmetry, and more generally, of any polytope generated as one orbit of any finite reflection group (Champagne *et al.*, 1995) in the real Euclidean space.

The simple roots of H_3 can be partially defined as follows:

The straight line containing $\pm\alpha_1$ passes through the centres of two opposite pentagons of the shell C_{60}.

The straight line containing $\pm\alpha_2$ passes through the centres of two opposite edges of C_{60} that separate two hexagons.

The straight line containing $\pm\alpha_3$ passes through the centres of two opposite hexagons of the shell C_{60}.

To complete the definition of the α-basis, one has to specify relative angles between the three roots α. Correct angles are crucial in defining the ω-basis that is dual to the α-basis [equation (4)]. Only in the ω-basis is the computation of the faces of dimension 0 (vertices), 1 (edges) and 2 relatively easy.

The icosahedral group H_3 underlies both the fullerenes and the aperiodic three-dimensional crystals ('quasicrystals') (Moody *et al.*, 2008; Moody & Patera, 1993). It is undoubtedly possible to link the fullerenes and nanotubes with suitably set up infinite quasicrystals. In our opinion a systematic investigation of such possibilities would be of interest.

The authors are grateful for partial support of this work by the Natural Sciences and Engineering Research Council of Canada and by the MIND Research Institute of Irvine, California. MS would like to express her gratitude to the Centre de Recherches Mathématiques, Université de Montréal, for the hospitality extended to her during her postdoctoral fellowship. She is also grateful to MITACS and to OODA Technologies for partial support. The authors would like to thank Dr M. Angelova for stimulating discussions and comments.

References

Cataldo, F., Iglesias-Groth, S. & Manchado, A. (2010). *Fullerenes, Nanotubes and Carbon Nanostructures*, **18**, 224–235.
Champagne, B., Kjiri, M., Patera, J. & Sharp, R. T. (1995). *Can. J. Phys.* **73**, 566–584.
Chen, L., Moody, R. V. & Patera, J. (1998). *Quasicrystals and Discrete Geometry*, Fields Institute Monograph Series, 10, edited by J. Patera, pp. 135–178. Providence: American Mathematical Society, Fields Institute.
Conway, J. & Sloane, N. (1998). *Sphere Packing, Lattices and Groups*, 3rd ed. New York: Springer.
Deodhar, V. V. (1982). *Commun. Algebra*, **10**, 611–630.
Dresselhaus, M. S., Dresselhaus, G. & Eklund, P. C. (1996). *Science of Fullerenes and Carbon Nanotubes.* San Diego: Academic Press.
Fowler, P. W. & Manolopoulos, D. E. (2007). *An Atlas of Fullerenes.* Mineola: Dover Publications, Inc.
Harris, P. J. F. (1999). *Carbon Nanotubes and Related Structures.* Cambridge University Press.
Humphreys, J. E. (1990). *Reflection Groups and Coxeter Groups.* Cambridge University Press.
Keef, T. & Twarock, R. (2009). *J. Math. Biol.* **59**, 287–313.
Kroto, H. W. & Walton, D. R. M. (1993). Editors. *The Fullerenes.* Cambridge University Press.
Li, H. & Xu, Y. (2009). *Math. Comput.* **78**, 999–1029.
Litvin, D. B. (1991). *Acta Cryst.* A**47**, 70–73.
McKenzie, D. R., Davis, C. A., Cockayne, D. J. H., Muller, D. & Vassallo, A. M. (1992). *Nature (London)*, **355**, 622–624.
Moody, R. V., Nesterenko, M. & Patera, J. (2008). *Acta Cryst.* A**64**, 654–669.
Moody, R. V. & Patera, J. (1992). *J. Phys. A: Math. Gen.* **25**, 5089–5134.
Moody, R. V. & Patera, J. (1993). *J. Phys. A: Math. Gen.* **26**, 2829–2853.
Moody, R. V. & Patera, J. (1995). *Can. J. Math.* **47**, 573–605.
Randic, M. & Vukicevic, D. (2006). *Croat. Chem. Acta*, **79**, 471–481.
Shinar, J., Vardeny, Z. V. & Kafafi, Z. H. (1999). Editors. *Optical and Electronic Properties of Fullerene-based Materials.* New York: Marcel Dekker.
Szajewska, M. (2012). arXiv:1204.1875v1 [Math.MG].
Twarock, R. (2002). *Phys. Lett. A*, **300**, 437–444.
Verberck, B. & Michel, K. H. (2007). *Phys. Rev. B*, **75**, 045419.